Astron. Astrophys. 339, 497–506 (1998)

ASTRONOMY AND ASTROPHYSICS

Doppler imaging of stellar surface structure

IX. A high-resolution image of the weak-lined T Tauri star HDE 283572 = V987 Tauri

K.G. Strassmeier[1,⋆] **and J.B. Rice**[2,⋆]

[1] Institut für Astronomie, Universität Wien, Türkenschanzstrasse 17, A-1180 Wien, Austria (strassmeier@astro.univie.ac.at)
[2] Department of Physics, Brandon University, Brandon, Manitoba R7A 6A9, Canada (rice@BrandonU.ca)

Received 21 July 1998 / Accepted 18 August 1998

Abstract. We present a Doppler image of the T Tauri star HDE 283572 from a set of high-quality spectroscopic line profiles and simultaneous multicolor photometry from October 1997. Additional photometry throughout the entire observing season was obtained with a robotic telescope and is used to determine the precise photometric period of 1.5495±0.0002 days that we interpret to be the stellar rotation period. Further relevant astrophysical parameters like mass, luminosity, radius, effective temperature, gravity, and elemental abundances are obtained and discussed. HDE 283572 shows one of the largest and coolest polar spots ever observed and confirms an earlier map by Joncour et al. from Pic-du-Midi data. We also compare our map with predicted magnetic flux-tube distributions from MHD simulations and suggest that the polar spot on HDE 283572 was possibly created by a strong poleward meridional flow.

Key words: stars: activity – starspots – stars: imaging – stars: individual: HDE 283572 – stars: late-type

1. Introduction: Surface imaging of T Tauri stars

The weak emission-line T Tauri stars – hereafter WTTSs – are recognized as the immediate precursors to main-sequence stars of spectral types A through M including our Sun. In one of the first studies on T Tauri stars, Joy (1945) noted a similarity of (classical) T Tauri emission-line spectra to that of the solar chromosphere. Photospheric spectra of WTTSs appeared "normal" in comparison with that of the late-type stars or even the Sun. It is now observationally well established that WTTSs exhibit the same phenomenological magnetic activity as rapidly rotating post-main-sequence stars, with possibly one – still lively debated – difference: magnetically controlled accretion of left-over circumstellar material onto the stellar surface (Bertout et al. 1988, Bouvier et al. 1995). The general picture is that classical T Tauri objects have accretion disks while WTTSs no longer have such disks and therefore WTTSs should not show signs of accretion anymore. The immediate question to be answered before we interpret spatially resolved data is, how can we discern between accretion spots and hot features such as chromospheric plages. Probably the most direct technique for doing this is to spatially resolve the stellar surface at appropriate optical depths by means of Doppler imaging. Another, no less interesting, goal of the present series of papers is to find evidence for or against the existence of cool spots situated directly at a star's rotation pole and whether they could be responsible for the angular momentum loss of young, ultra-rapidly rotating, late-type cluster stars (Solanki et al. 1997) as well as in the case of single, or effectively single, field G–K giants (Strassmeier et al. 1998).

Doppler imaging is an elaborate observational and computational technique similar to medical tomography and inverts a series of high-resolution spectral line profiles into an "image" of the stellar surface (e.g. Vogt et al. 1987, Rice et al. 1989, Collier Cameron 1992, Piskunov & Rice 1993). The few existing Doppler maps of pre-main-sequence stars generally do not exhibit a cap-like polar spot such as we see with most evolved RS CVn-type stars, e.g. HR 1099, UX Ari, HU Vir, EI Eri (a.o., for references see the listing in Strassmeier 1996). Only the Doppler map of the WTTS HDE 283572 by Joncour et al. (1994a) from Pic du Midi data in February 1993 showed precisely this sort of cool, polar cap-like spot with the large temperature difference of 1,600 K, but not a single equatorial feature! Doppler maps of the G-star component of the young, double-lined spectroscopic binary HD 155555 by Kürster et al. (1992), Dempsey et al. (1999) and Hatzes & Kürster (1999) also showed a polar cap-like spot but the evolutionary status of HD 155555 – evolved or pre-main sequence – is not completely agreed upon despite relatively strong lithium lines from both components. On the WTTS V410 Tau, Strassmeier et al. (1994) and Rice & Strassmeier (1996) found spots at both equatorial latitudes and at very high latitudes with the high-latitude spots being cooler and larger and having greater longevity than the equatorial spots. This was confirmed by Hatzes (1995) and seems also to be in accordance with the polar feature found earlier by Joncour et al. (1994b). Two recent images of the very young (few 10^5 years) run-away WTTS V1321 Ori (Par 1724) in the Orion association by Neuhäuser et al. (1998) and Stout-Batalha (1997) showed

⋆ Visiting Astronomer, Canada-France-Hawaii Telescope, operated by the National Research Council of Canada, the Centre National de la Recherche Scientifique de France, and the University of Hawaii

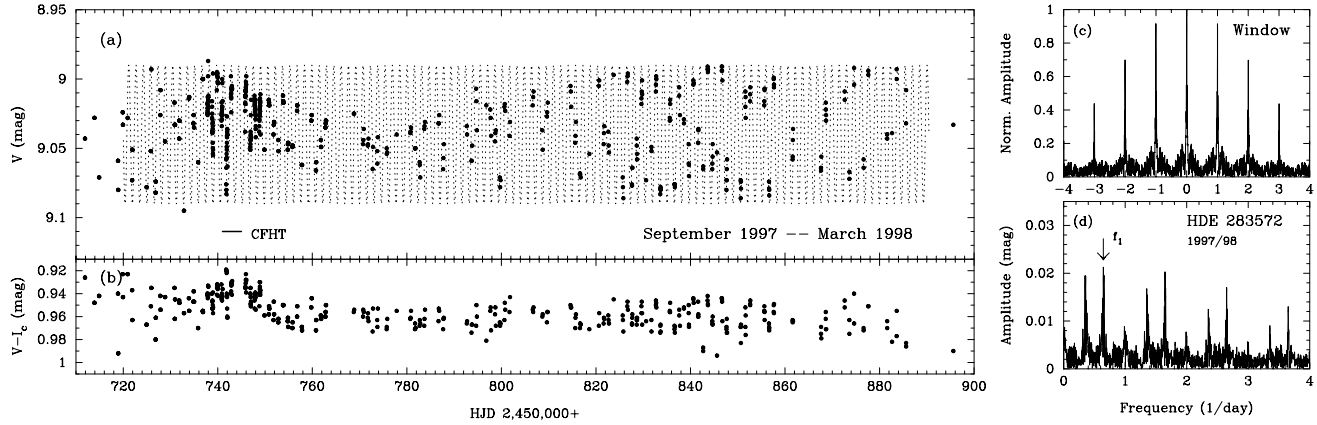

Fig. 1. a The V magnitude observations during the entire observing season 1997/98 (170 nights) and, in panel **b**, the V-I color variations. The horizontal bar in panel **b** indicates the time of the Doppler-imaging observations at CFHT while the dotted line is a sinusoid with the best-fit photometric period and constant amplitude. Note that the V-I amplitude increases with increasing V amplitude. This, and the fact that the star becomes redder when fainter, is in agreement with a cool starspot model. The periodogram in panel **d** from the combined V and y-band data indicates $P_{\rm phtm}$=1.5495 days (indicated as f_1). Panel **c** shows the window function with aliasing periods centered around multiples of one day.

mostly low-to-moderate latitude activity with one feature extending close to the pole but not a polar cap. Further, once a veiling map had been subtracted, Doppler images of the classical T Tauri objects DF Tau (Unruh et al. 1998) and SU Aur (Petrov et al. 1995) displayed cool spots predominantly near the stellar equator but not near their respective rotation poles. Not so on Sz68 though, a classical T Tauri star without detectable veiling, where Johns-Krull & Hatzes (1997) found a large polar cap-like spot and also evidence for magnetospheric accretion onto the stellar surface.

In order to understand such a variety of spatially-resolved information, we felt that further Doppler maps of T Tauri stars are needed and have been collecting data to Doppler image the WTTS HDE 283572 with spectra of superior resolution, signal-to-noise, and phase coverage. HDE 283572 = V987 Tauri is embedded in the young (few 10^6 years) Taurus-Auriga T association and Walter et al. (1987) first drew attention to this star and presented a detailed discussion of observations at wavelengths ranging from X-ray to the near infrared. Just recently, Donati et al. (1997) presented a marginally significant but nevertheless direct detection of a magnetic field on HDE 283572 and thus confirmed the nature of the star's activity. In Sect. 2 in this paper we first present the new photometric and spectroscopic observations and the respective instrumentations and in Sect. 3 we determine the absolute stellar parameters of HDE 283572. Sect. 4 presents the results of our Doppler-imaging analysis, and Sect. 5 summarizes our discussion and conclusions of this paper.

2. New observations

2.1. Photometry

Continuous photometry was obtained between November 1996 and March 1998 with Wolfgang and Amadeus, the two 0.75m Vienna Observatory Twin Automatic Photoelectric Telescopes (APT), (Strassmeier et al. 1997a) at Fairborn Observatory in Washington Camp in southern Arizona (the monitoring is still being continued). This sequence was sampled with up to three measures in every clear night, each the mean of three readings of the variable and the comparison star. During a 10-day interval in October 1997 – centered at the mid time of our spectroscopic observations – both APT's monitored HDE 283572 throughout the night. Wolfgang was equipped with b and y Strömgren filters while Amadeus measured in Johnson-Cousins VRI and the narrow (30 Å) Hα filter. Altogether, 845 data points were acquired between 1996–1998, but only the 1997/98 season data (459 useable data points) are analysed in this paper (Fig. 1). The standard error of a nightly mean from the overall seasonal mean for the Amadeus-APT data significantly improved after mid 1997 and was thereafter – for both APTs – 2.5 millimag in V (and b and y) and 4 millimag in R_c and I_c. The rms error for the narrow Hα-filter data are twice as large due to the lower count rate.

Our initial comparison star (=C1=HD 27570, see Table 1) turned out to be slightly variable and showed occasional flaring with up to $0\overset{\rm m}{.}05$ in V and possibly a 20-day periodic 0.005-mag modulation. After JD 2,450,828 we added a new comparison star, a new check star, and a new navigation star but kept the initial group as well since its check star (Ck1) remained constant. Table 1 summarizes the magnitudes and color indices of HDE 283572 and all the reference stars. The V and y-band data from 1997/98 are plotted in Fig. 1a with respect to check star Ck1 as well as versus comparison star C2 after JD 2,450,828. The V amplitude varied between $0\overset{\rm m}{.}02$ in November 1997 and a maximum value of $0\overset{\rm m}{.}10$ in February 1998. Fig. 1b shows the V-I_c colors throughout the observing season with a maximum amplitude of $0\overset{\rm m}{.}035$ coinciding with the maximum V amplitude in around February 1998. Note that at this time the star was brightest, while it appeared faintest (with a difference of $0\overset{\rm m}{.}05$) during the times of low amplitude. Such a behavior is contrary to what is usually observed for spotted stars where a fainter state

Table 1. Photometric indices for HDE 283572 and its comparison and check stars

Star	V	(B-V)	(V-I$_c$)
HDE 283572[a]	8.992	[0.780±0.007]	0.932±0.01
HDE 283572[b]	9.02	0.798±0.025	0.83±0.02
HDE 283572[c]	9.04	0.83±0.01	0.94±0.01
HD 27570[b] (C1)	9.09	0.656±0.004	0.72±0
HD 28447[b] (Ck1)	6.51	0.722±0.007	0.77±0.01
HD 27741[b] (C2)	8.31	0.642±0.007	0.71±0.01
HD 282183[a] (Ck2)	9.26	...	0.68±0.02

[a]This paper (brightest=unspotted values are given), [b]ESA (1997), [c]Walter et al. (1987). A (B-V) entry in brackets is actually (*b*-*y*).

Table 2. Astrophysical data for HDE 283572

Parameter	Value
Spectral type	G5(IV)
Distance (Hipparcos)	128±18 pc
$M_{\rm V}$	+3.45±0.29 mag
Luminosity	3.3±1.0 $L_\odot$
$\log g$	3.5±0.5
$T_{\rm eff}$	5250±100 K
A_V	$0.3^{+0.2}_{-0.1}$ mag
$v \sin i$	78.0±1.0 km s^{-1}
Photometric period	1.5495±0.0002 days
Minimum radius $R \sin i$	2.39±0.03 $R_\odot$
Inclination	$35^{\circ\,+15}_{-5}$
Mass	1.8±0.2 $M_\odot$

means more spots on the surface and thus larger light modulation and a brighter state less spots and thus less modulation. The opposite behavior of HDE 283572 indicates that the overall light level must be dominated by a rotationally unmodulated spot component, e.g. a polar spot or a homogeneous spot distribution along stellar longitude.

2.2. Spectroscopy

All spectroscopic observations in this paper were obtained with the Gecko Coudé spectrograph at the 3.6-m Canada-France-Hawaii telescope (CFHT) in October 19–23, 1997. The 2048^2 Loral-5 CCD with 15μm pixels and the dispersion of 1.6 Å/mm provided a resolving power of 120,000 (2.5 km s^{-1}) in a useful wavelength range of around 50 Å centered at 6710 Å. Seeing was always between 0.6–1.2″ and all integrations were set at an exposure time of 5×10 min and have typical signal-to-noise ratios of 170:1. This sequence allowed for a total of 27 spectra well distributed over all rotational phases. Fig. 3 displays a typical spectrum. No water-vapor lines above the nominal noise level are obvious in these spectra and no attempts were made to correct for it. The reduction procedure was identical to that in our recent paper on LQ Hydrae (Rice & Strassmeier 1998) obtained with the same telescope and instrumental set up and we refer the reader to that paper.

The high spectroscopic resolving power combined with the large rotational broadening of HDE 283572 ($v \sin i$=78 km s^{-1}) allows for an unprecedented 60 resolution elements across the stellar equator or a spatial resolution of approximately 1°. However, the exposure time of 50 min will cause phase smearing of up to a maximum of 10° along the equator and in the direction of the rotational motion.

3. Absolute parameters for HDE 283572

3.1. Brightness and luminosity

The trigonometric parallax from Hipparcos (ESA 1997) converts to a distance of 128±18 pc and with the brightest, i.e. presumably unspotted, V magnitude of $8\overset{\rm m}{.}992\pm0\overset{\rm m}{.}005$ observed in early 1998, the absolute visual magnitude is $M_{\rm V} = +3\overset{\rm m}{.}45 \pm 0\overset{\rm m}{.}29$. Interstellar absorption was adopted from E(B-V)$\approx 0\overset{\rm m}{.}1$ (Walter et al. 1987) to be $A_V = 3.2 E_{\rm B-V} \approx 0\overset{\rm m}{.}3^{+0.2}_{-0.1}$.

An absolute magnitude of $\approx+3\overset{\rm m}{.}5$ clearly indicates that the star is not on the main sequence and suggests a luminosity class appropriate for a subgiant. The dereddened Hipparcos B-V color of $\approx0\overset{\rm m}{.}7$ (where we assume no error on E(B-V)=0.1) indicates a G5IV star with $T_{\rm eff}$ of 5600 K according to the tables of Gray (1992) or 5560 K according to the more recent color-temperature transformation of Flower (1996). With B.C.=−0.124 from Flower (1996) the bolometric magnitude is $+3\overset{\rm m}{.}33$, and with $M_{\rm bol,\odot} = +4\overset{\rm m}{.}64$ (Schmidt-Kaler 1982) the luminosity of HDE 283572 is estimated to be 3.3±1.0 $L_\odot$ (Table 2). A comparison with the most recent pre-main-sequence evolutionary tracks from D'Antona & Mazzitelli (1997) suggests a mass of 1.8±0.2 $M_\odot$. Fig. 2 shows the position of HDE 283572 in the theoretical H-R diagram.

3.2. Photometric period

The photometric period of HDE 283572 was first determined by Walter et al. (1987) to 1.548 days from a comparably rather small set of photometry in 1983. It is, however, in excellent agreement with our new and much more precise period from 1997/98, i.e. 1.5495±0.0002 days. The APTs gathered 456 data points with $\sigma \leq 0.01$ within six months and Fig. 1 shows these data and the periodogram from a least-squares Fourier analysis. The error of the period is estimated from the width of the frequency peak with the smallest χ^2 at $\chi^2_{\rm min} + (\chi^2_{\rm min}/(n-m))$ where n is the number of data points and m the number of parameters ($n-m$ is then the number of the degrees of freedom; $m = 4$ in our case).

This period is only marginally different from that used in previous studies but nevertheless large enough so that phase coherence is lost within four years. All line profiles and photometric data are phased with our new photometric period that we interpret to be the stellar rotation period,

$$HJD = 2,450,395.0 + 1.5495 \times E, \quad (1)$$

where the initial epoch is just an arbitrary point in time and coincides with our first APT measure in late 1996.

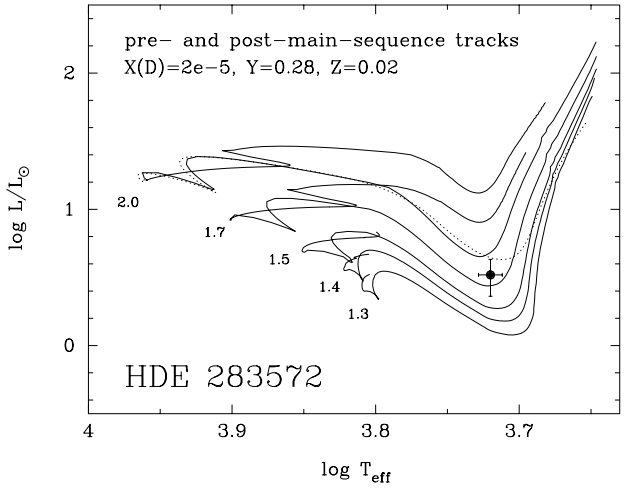

Fig. 2. The position of HDE 283572 in the H-R diagram. The solid lines are the combined pre- and post-main-sequence tracks of D'Antona & Mazzitelli (1997) for masses of 1.3, 1.4, 1.5, 1.7, and 2.0 solar masses. For comparison, the old 2.0-$M_\odot$ pre-main-sequence track from D'Antona & Mazzitelli (1994) is plotted as a dotted line in order to estimate the significance for HDE 283572. The differences are due to changes in the equation of state, opacities, and the convection treatment.

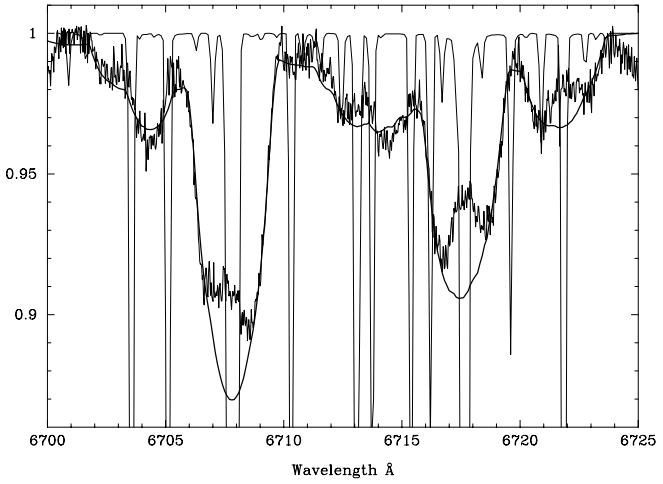

Fig. 3. Spectrum synthesis of the Li I line at 6707.8 Å and the Ca I line at 6717 Å. The lithium abundance is essentially primordial, Ca is overabundant by 0.4 dex and Si by 0.5 dex. The thin line is the unbroadened synthetic spectrum to demonstrate the amount of blending. The fit to an observed spectrum with $v \sin i$=78 km s^{-1} is shown as a thick line. Note the large line-core filling of up to 3.5% of the continuum, i.e. one third of the line depth.

3.3. Rotational broadening and the stellar radius

$V \sin i$ was determined from the 6690–6740 Å wavelength region shown in Fig. 3. We assumed an instrumental profile approximated by a Gaussian profile with the FWHM from several unblended Th-Ar comparison lines and deconvolved this from the data. The transition probabilities in this wavelength region were partly modified by first fitting the solar spectrum and the modifications are listed in Table 3. Macroturbulence was implicitely accounted for by the integration over the visible hemisphere of Doppler-shifted local line intensities. A model with $v_{\rm macro}$=4 km s^{-1} and $v_{\rm micro}$=2 km s^{-1} was adopted for HDE 283572. The resulting value for $v \sin i$ is 78.0±1.0 km s^{-1} and is in good agreement with a previous determination by Donati et al. (1997) of 77±2 km s^{-1}. The large values of 95 and 130 km s^{-1} obtained by Walter et al. (1987) from comparably low-resolution data are now clearly obsolete. Joncour et al. (1994a) adopted an unprojected equatorial rotational velocity of 90 km s^{-1} ($v \sin i$ or error bars were not given) and an inclination i of 60° for their Doppler imagery in 1993.

If our photometric period is assumed to be the stellar rotation period, which is the general rule for spotted stars, the value of $v \sin i$=78±1.0 km s^{-1} would confine the stellar radius to values larger than 2.39±0.03 $R_\odot$. As a comparison, the radius from the bolometric-luminosity – effective-temperature relation from the Hipparcos data discussed in Sect. 3.1 is 2.21±0.35 $R_\odot$. We will show later in Sect. 4 that the range of plausible inclinations of the stellar rotation axis is between 30–50° and the unprojected radius should therefore be between 3.1–4.7 $R_\odot$. This gives a difference of at least 30% compared to the Hipparcos-based radius, a discrepancy that must be seen as significant since the best inclination from the Doppler imagery is found to be 35°, which translates to a best radius of 4.1 $R_\odot$, a result that should be reliable since the error bars on the photometric period and $v \sin i$ are very small. A possible explanation could be that, first, the observed photometric period is the rotation period of the star at very high latitudes and if the star is differentially rotating the equatorial rotation period could be different by up to 10% as in the case of the Sun and, second, the effective temperature in the luminosity-temperature relation must be replaced by an average surface temperature which is lower by ≈300 K.

Table 3. Atomic data and line equivalent widths

Line	$\log gf$	χ	W_λ (mÅ)		
	(–)	(eV)	ϵ Eri	11 LMi	HDE
Fe I 6703.568	–3.50	2.759	53	58	b
Fe I 6705.101	–1.45	4.607	56	69	b
Fe I 6705.131	–2.36	4.956	b	b	b
Li I 6707.761	–0.10	0.000	≤3	≤3	287
Li I 6707.912	–0.36	0.000	b	b	b
Fe I 6710.316	–5.05	1.485	34	37	b
Fe I 6713.046	–1.80	4.607	32	48	b
Fe I 6713.195	–2.69	4.143	20:	17:	b
Fe I 6713.745	–1.69	4.795	25	38	b
Fe I 6715.383	–1.81	4.608	35	50	b
Ni I 6716.128	–4.50	1.951	b	b	b
Fe I 6716.225	–2.09	4.580	21	32	b
Fe I 6717.524	–1.82	4.607	b	b	b
Ca I 6717.681	–0.85	2.709	154	150	197
Si I 6719.609	–2.00	6.206	8	26	b
Si I 6720.903	–2.85	5.871	4	8	b
Si I 6721.848	–1.47	5.863	31	67	b

Notes: "b" = blend; ":" = from a two-Gaussian fit. The given W_λ(Li) is for the combined ^{6}Li and ^{7}Li lines.

3.4. Effective temperature, gravity, and lithium abundance

Detailed LTE synthesis of our R=120,000 spectra is used to determine the lithium abundance, the effective temperature, and the gravity of HDE 283572. For elements not otherwise noted, solar abundances from Grevesse & Anders (1991) were used for the synthesis. Model atmospheres are taken from the grids provided by Kurucz (1993) and include our own updated atomic line list from previous papers in this series. With the new modifications for the 6700-Å wavelength region in Table 3 we computed synthetic spectra from a grid of ($T_{\rm eff}$,$\log g$)-atmospheres with 4750, 5000, 5250, 5500, and 5750 K and 3.0, 3.5, and 4.0, respectively. Microturbulence was always assumed to be 2.0 km s^{-1}. The best fit from the 6690–6740 wavelength region in Fig. 3 is obtained with the 5250/3.5 atmosphere. Typical uncertainties are in $T_{\rm eff}$ $\pm$100 K, in $\log g$ $\pm$0.25, and for the abundances of the prominent elements approximately $\pm$0.1 dex. Significant overabundances relative to the solar values of Grevesse & Anders (1991) for Ca (+0.4 dex) and Si (+0.5 dex) are needed for all trial models.

The Kurucz (1993) $\log gf$ values for ^{6}Li and ^{7}Li are -0.009 and -0.309, respectively but synthetic spectra for the 6708-Å region of the Sun (G2V), ϵ Eri (K2V), and 11 LMi (G8IV-V) result in overall better fits when using -0.102 and -0.360. The wavelengths and transition probabilities for the ^{12}CN feature at 6707.529 and the Fe I 6707.443 line that both blend with the Li I line were taken from Gilroy (1989). In this way, and under the assumption of LTE, we would obtain a Li abundance of $\log n$(Li)=3.5$\pm$0.2 (on the $\log n$(H)=12.00 scale), which exceeds the primordial value of a Pop I star (3.2–3.3). When using the LTE and the non-LTE curves of growth of Pavlenko & Magazzú (1996) for a 5250/3.5 model and our average equivalent width of 287$\pm$9 mÅ we get Li abundances of 3.3 and 3.2 from the LTE and the non-LTE curves, respectively. Such consistently high values indicate that the cool starspots on HDE 283572 have some influence on the measured Li equivalent width, most likely due to the lower local surface temperature and possibly also due to a lower gravity within the spot (Saar et al. 1995). Our final lithium abundance is thus determined from the Doppler imaging analysis once the spot temperature and their distribution has been determined from another chemical element (calcium in our case). This value is $\log n$(Li)=3.35$\pm$0.10, and is in good agreement with the previously obtained value from the line equivalent width but smaller by 0.15 dex than the values from the synthetic spectra. Although we do not consider this as a significant difference it nevertheless suggests smaller lithium abundances for spotted stars once the temperature inhomogeneities were taken into account but the abundance for HDE 283572 is still at the upper limit of the primordial value.

Soderblom et al. (1993) and others have already pointed out that the Li abundance of a heavily spotted star could appear higher by a few dex when cool spots are in view. Unless there are cool spots in sight all the time, e.g. a polar spot, we would expect to see some rotational modulation of the Li equivalent width, which we do not. Actually, our line measures indicate a rather constant equivalent width of 287 mÅ with a standard deviation of just 9 mÅ, comparable to the deviation for the nearby Ca I 6717-Å line (197$\pm$10 mÅ). This is suggestive of the existence of a rotationally unmodulated spot component, again e.g. a polar spot, because lithium is very temperature sensitive and thus especially prone to rotational modulation. Rotational modulation of the lithium equivalent width was only recently detected for the spotted WTTS V410 Tau by Fernández & Miranda (1998) and for P1724 by Neuhäuser et al. (1998), but both of these stars have comparably much larger photometric variations and no prominent polar spot.

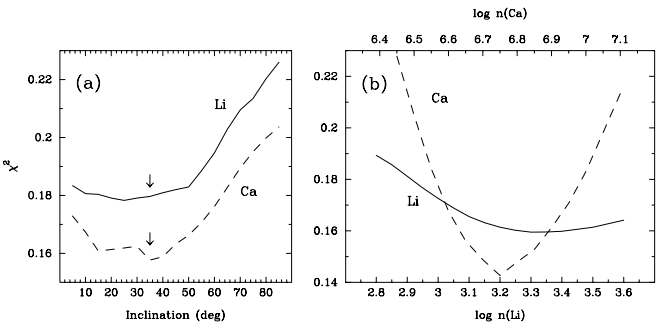

Fig. 4a and b. The quality of the line-profile fits for **a** various inclinations of the stellar rotation axis and **b** various abundances for lithium and calcium at a fixed inclination of 35°. The full and dashed lines are for Li I 6707 and Ca I 6717, respectively. Both spectral lines indicate an overall minimum of the combined χ^2 with $i \approx 35°$ (arrows) and abundances of $\log n$(Ca)=6.75 and $\log n$(Li)=3.35, respectively. These are the values adopted for the Doppler imaging. Note that for inclinations lower than 15° the equatorial velocities would approach the break-up velocity of the star and are thus fictious.

3.5. Space-motion components

With the Hipparcos parallax and the average radial velocity of 15$\pm$2 km s^{-1} from various authors and our own spectra we redetermine the (U,V,W) space-motion components relative to the Sun in a right-handed coordinate system to be -15.1 ± 2.3, -12.9 ± 1.9, -11.4 ± 0.5 km s^{-1}. These velocities place HDE 283572 well within the Taurus-Aurigae velocity dispersion of the Frink et al. (1997) sample who adopted the pre-Hipparcos distance of 140 pc (Kenyon et al. 1994). Note that the cloud's distance obtained from the mean velocity dispersion is 125$\pm$39 pc and is smaller than but consistent with the 152$\pm$10 pc recently obtained by Preibisch & Smith (1997) on the basis of rotational properties of 25 WTTS and also in excellent agreement with the Hipparcos distance of 128$\pm$18 pc. The new Hipparcos parallax and above UVW-space motions place HDE 283572 into the central part of the cloud and thus further strengthen its pre-main-sequence status.

4. A Doppler image for October 1997

The Doppler imaging program used here is based on the original code of Rice et al. (1989) developed for Ap-star mapping. In the course of this series of papers, several significant modifications were made to the original code and these were partially

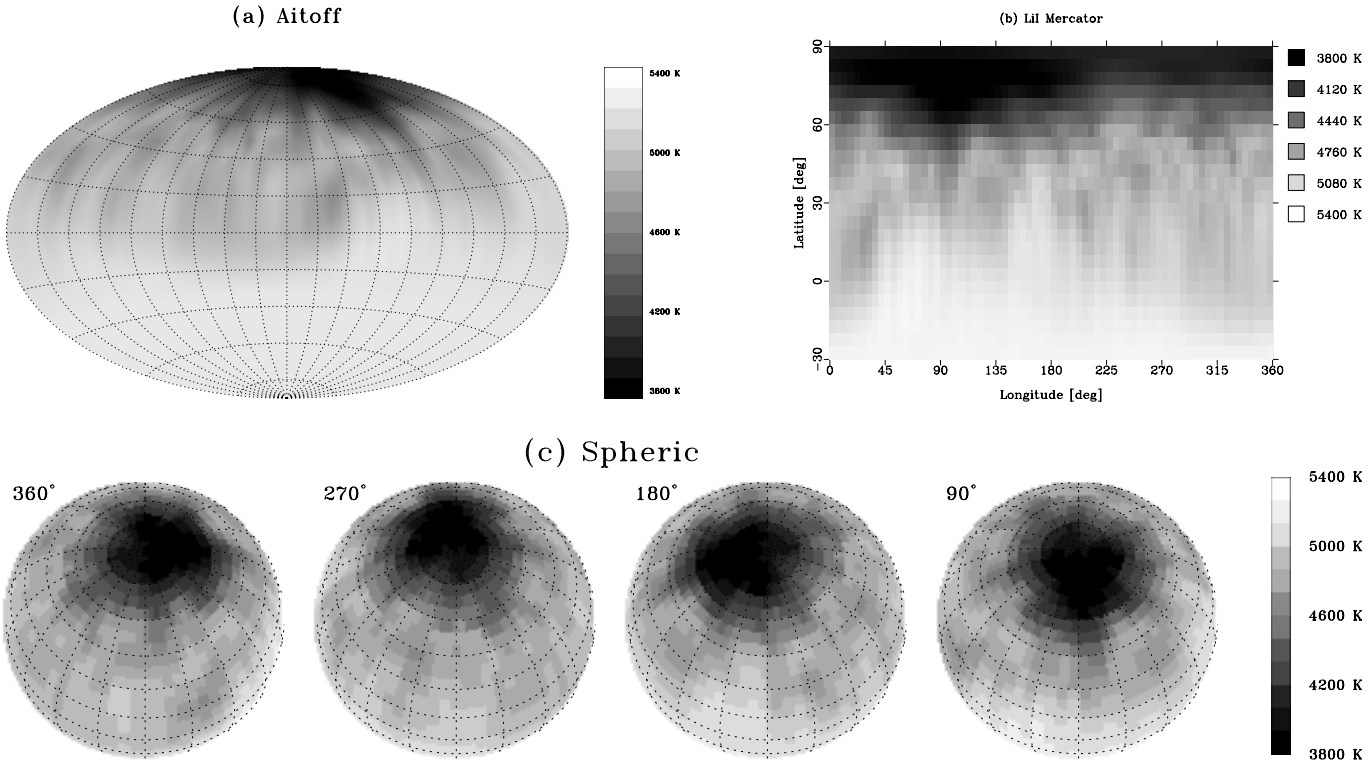

Fig. 5a–c. Doppler images of HDE 283572 from Li I 6707 Å. Maps are plotted in three different projection styles, from top to bottom, in **a** a true-area Aitoff projection, **b** a pseudo-Mercator projection and, **c** in a more realistic spherical projection at four equidistant rotational phases. The temperature scale is indicated and is the same for all projections. The central meridian in the Aitoff map is zero longitude.

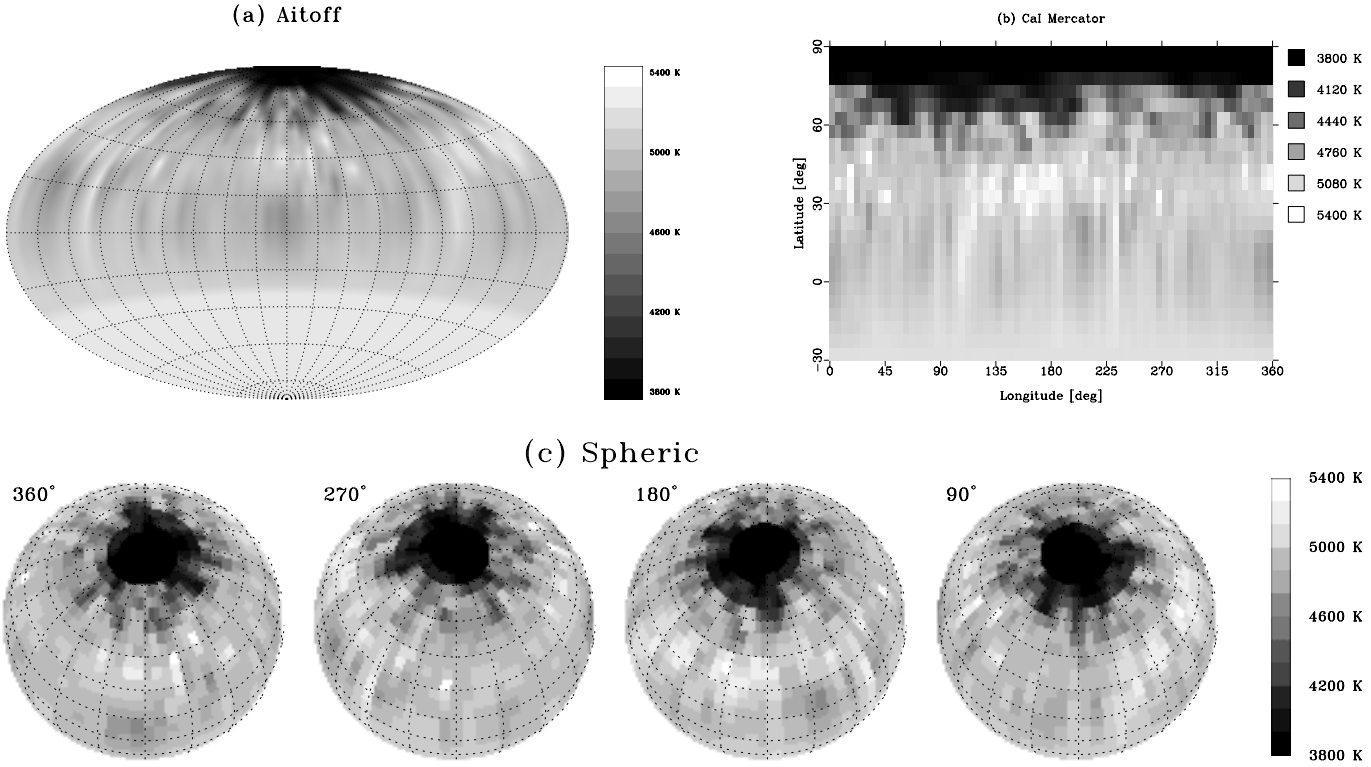

Fig. 6a–c. Doppler images of HDE 283572 from Ca I 6717 Å. Otherwise as in Fig. 5a–c.

described in Piskunov & Rice (1993), Rice (1996), Strassmeier & Rice (1998) and Rice & Strassmeier (1998), and for details we refer the reader to these papers. For HDE 283572, our procedure includes a full spectrum synthesis via a solution of the equation of transfer through a set of pre-tabulated Kurucz (1993) model atmospheres with 72 depth points and for effective temperatures between 5,750 and 3,500 K and for each of the observed wavelength regions at all limb angles. Simultaneous inversion of up to twenty line blends as well as two photometric bandpasses using either a maximum-entropy or a Tikhonov regularisation is possible. For this paper we chose the V and R, and the V and I bandpasses and the maximum-entropy regularisation. All computations were performed on a DEC Alpha 500 workstation and required on average 30 CPU-minutes for one run with 11 blends and 15 iterations.

We run numerous solutions to predetermine the best inclination of the stellar rotation axis as well as the chemical abundances of the elements of the two main mapping lines. Fig. 4a shows the quality of the combined line profile and light curve fits versus trial inclinations from 5° to 85°. Clearly, only low inclinations yield a significant reduction of the χ^2. While there is a formal minimum for both spectral regions, it is usually fairly broad and not well defined so that we adopt a weighted average of 35° but emphasize that inclinations up to 50° are possible. Lower inclinations than 30° are more unlikely because the projected rotational velocity is already 78 km s^{-1}. For this paper we adopt an inclination of 35°. The right panel of Fig. 4a and b shows the χ^2 distribution versus a number of trial abundance values for Ca (top axis) and Li (bottom axis) at a fixed inclination of 35°.

Fig. 5a–c and Fig. 6a–c show the Doppler images from Li I 6707 Å and from Ca I 6717 Å, respectively. Both images are plotted in three different projection styles, where the pseudo-Mercator projection emphasizes the longitudinal distribution of surface features while the spherical projection suggests the relative importance of low and high-latitude features, and the Aitoff projection restores the correct area perspective. The line-profile fits are shown in Fig. 7 and the relevant photometric V, V-R, and V-I fits are shown in Fig. 8 along with the observations.

Both maps reveal a cool polar spot covering approximately 6% of the entire stellar surface. Its average temperature from both spectral lines is 3800±100 K, thus 1450 K cooler than the unspotted photosphere. The very coolest parts of the polar spot show some significant differences from the two images in that the part from Li appears more asymmetric with respect to the stellar rotation pole than the part from Ca. The overall shape and the position of the individual appendages agree very well within the two lines but the Li line recovers a slightly larger feature than the Ca line. This difference is 5% for temperatures of up to 4000 K, 15% for up to 4400 K, and 35% for up to 4800 K. This is not unexpected because the large temperature sensitivity of the Li line with its zero low-excitation potential tends to emphasize the cooler features relative to the warmer features. The Ca line, on the other hand, has a lower excitation potential of 2.7 eV. Also, the Li line is a very close blend of the two isotopes ^{6}Li and ^{7}Li and mimics a broad local line profile which, in turn, results in a lower surface resolution. This is readily seen in the maps in Figs. 5a–c and 6a–c. Additional uncertainties due to uncertainties of the isotopic $\log gf$'s with respect to a single unblended line, like the Ca line, can be expected. There is nevertheless an astonishing amount of corresponding detail in the two maps, as can be seen from a comparison of Figs. 5a,b,c and 6a,b,c.

The appendages of the polar spot are too numerous to be discussed individually (eight strong ones are consistently recovered from both lines). The strongest one is seen at a longitude of approximately 90° and reaches to a lower-latitude bound of nearly +30° in the Li map and +40° in the Ca map. While the latitudinal extent of spots in surface regions that are only briefly in view is certainly artificial, i.e. in regions south of the equator and the equatorial region themselves, it is certainly not true for the crown-like arrangement of the polar appendages. The apparent symmetry of the appendages of the polar "crown" creates the impression that there is some physical link to lower latitudes. Two hypothesis could be envisioned here: Equatorial spots either migrate polewards and merge with the polar spot to form the appendages as suggested by Vogt et al. (1998) and Vogt & Hatzes (1996) for HR 1099 or, the appendages separate from the polar spot and are about to migrate equatorwards. From a single image one can not discern between the two scenarios, it would require at least two images taken within, say, ten stellar rotations.

Do we see equatorial spots on HDE 283572 at all? Both maps contain some evidence for two (weak) low-latitude features. The larger of them is located at a longitude of 0° in the Ca map but at 30° in the Li map. Their respective areas and latitudes are ≈2% and between +(0–30)°. The Ca map shows an additional, though much smaller, feature at 30° longitude at the same position as in the Li map but it remains uncertain whether this feature is significant at all. The average temperature difference of these little spots is consistently around 400 K cooler than the adopted photospheric temperature. Note also that the light and color curves show a minimum at almost exactly 0° longitude (i.e., zero phase in Fig. 8) and the equatorial spots could be demanded by the photometry. A test inversion without photometry, however, even slightly enhances these spot's contrasts and verifies that they are are required by the line profiles, even the very small feature at 30° longitude in the Ca map. The second low-latitude feature is located at a longitude of 205±5° in both maps. Its central latitude is between +(20–30)° and differs by less than 10° in the two maps. Its contrast is similar to the other equatorial feature.

5. Discussion and conclusions

Our Doppler image of HDE 283572 shows a large and very cool polar spot with appendages extending almost symmetrically to a lower latitude bound of 50°. There is some evidence for two, comparably rather weak low-latitude features, but dominant equatorial or low-to-mid latitude spots are not existent. As such it is extreme within the zoo of Doppler imaged stars but in agreement with an earlier map obtained by Joncour et al. (1994a)

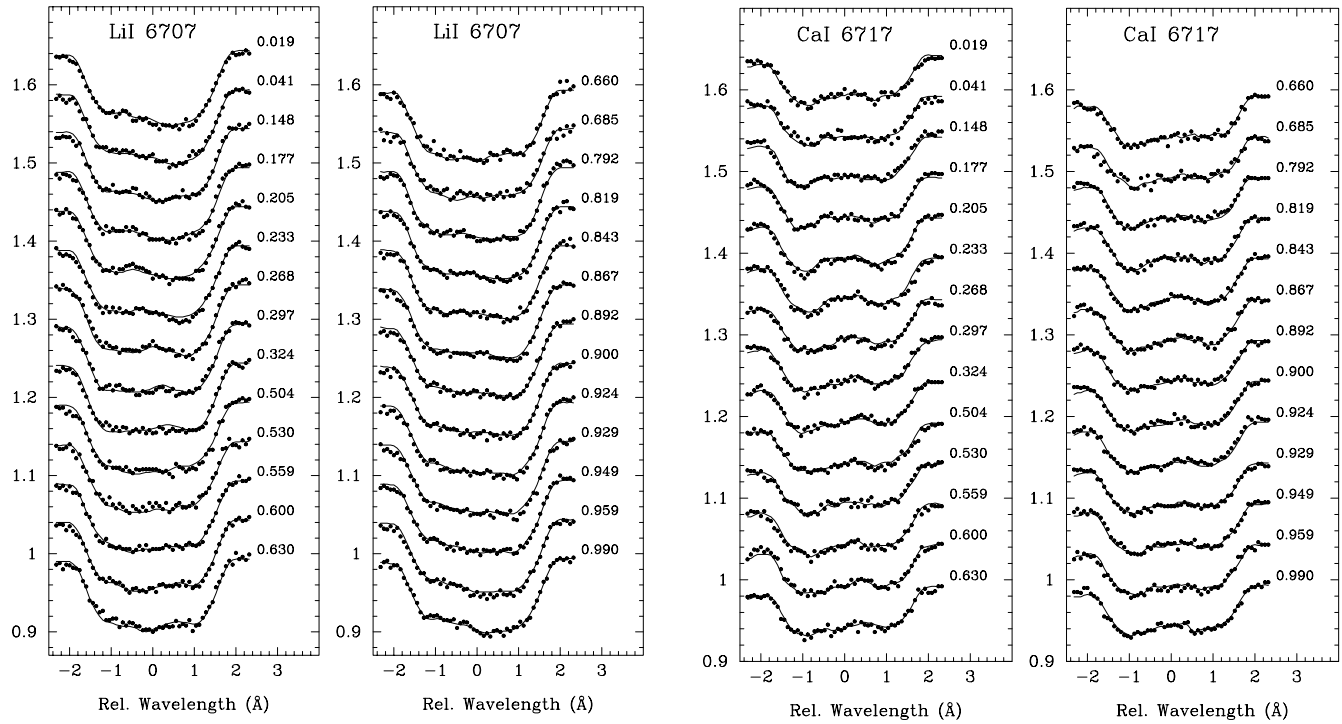

Fig. 7. Observed and computed line profiles for the two spectral lines. Top, the Li I 6707 line and, bottom, the Ca I 6717 line. The dots are the observations and the lines are the fits. Rotational phase is indicated on the right side of each profile. All observations were taken within four consecutive nights.

from comparably lower quality data. The surface temperature difference of this polar spot is 1450 K from the two spectral regions in agreement with our modeling of simultaneous $V(RI)_c$ light and color curves and is also compatible with the 1600 K obtained by Joncour et al. (1994a). It is entirely possible that the polar feature seen by Joncour et al. in 1993 is the same as what we find in October 1997. We note though that the time scale for the existence of any spot pattern is an uncertainty that cannot be resolved on the basis of even annual Doppler maps but there is abundant evidence that polar spots are long lived (e.g. Vogt & Hatzes 1996, Vogt et al. 1998). Long-term changes in multicolor photometric data of these objects could be decisive in this case and continuous monitoring is already underway using automatic photoelectric telescopes since the early eighties (e.g. Strassmeier et al. 1997b, Henry et al. 1995).

The existence of a prominent polar spot along with the absence of (significant) low-latitude features indicates a predominantly non-solar magnetic flux behavior. If we adopt the Caligari et al. (1995) MHD code and a model of the solar convection zone and spin it up to the rotation period of HDE 283572, we would expect to see magnetic flux only above a latitude of approximately 27° and no spots below that latitude, i.e. near the equator (c.f. Schüssler et al. 1996). If we compute an appropriate pre-main-sequence model matching the observed parameters of HDE 283572 with $\Omega = 17 \times \Omega_\odot$ and under MLT as outlined in Granzer et al. (1999), the lower latitude bound of the flux-tube emergence rises only marginally to 32°. Fig. 9 shows such a model with the corresponding trajectories of rising flux tubes. Given the very strong polar cap feature, it is obvious that the predicted flux emergence is still not in full agreement with the observed spot distribution in Fig. 6a–c and Fig. 5a–c even though the observations do not show dominant low-to-mid latitude spots as predicted by the Schüssler et al. (1996) model. We note that even tripling the stellar angular velocity will not lead to exclusively very high latitude flux tubes because of the existence of a mid-latitude stability island of the field strengths in the overshoot region. Within this stability region the corresponding flux tubes can remain for a longer time than usual and the dynamo has more time to strengthen the magnetic field and thus causes an almost radial flux trajectory and consequently some low-to-mid latitude flux loops. Within the framework of the Schüssler et al. (1996) model, the only two possibilities for explaining the observed HDE 283572 map are either to assume a strong poleward oriented meridional flow or, second, to enlarge the depth of the convection zone by almost a factor of two and assume that high-latitude rings of flux tubes continue to slip polewards once they have left the overshoot region (for a more thourough discussion of this "poleward slip" see, e.g., Caligari et al. 1995). Needless to say, the latter possibility would be in strong disagreement with the stellar model of HDE 283572, which predicts a depth of the convection zone of around 0.60 stellar radii. We thus suggest that HDE 283572 more likely exhibits a strong meridional flow toward the visible rotation pole, which supports DeLuca et al.'s (1997) conclusion that differential rotation and meridional flows in solar-like stars could be of greater importance than originally thought. Such a conclusion

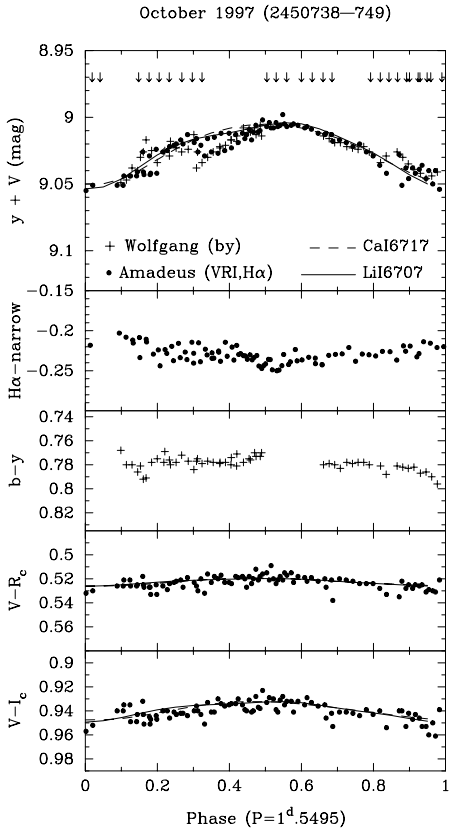

Fig. 8. Observed and computed light and color curves. The dots and plusses are the APT observations between October 15–29, 1997 and the lines are the fits from the Doppler-imaging analysis. Note that the Hα light curve is in antiphase indicating that chromospheric plages are spatially related to the appendages of the polar spot. The vertical arrows in the upper panel emphasize the phase coverage of our spectra.

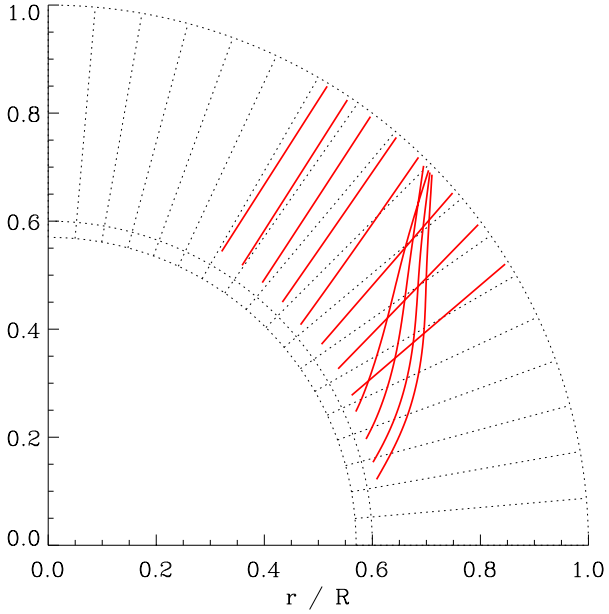

Fig. 9. The predicted latitude distribution of emerging flux tubes for a stellar model matching HDE 283572. The figure shows a radial cross section with the trajectories of the summit of rising flux loops. The small sector below the convection zone indicates the width of the overshoot region between r/R=0.57-0.60. The stellar model was computed under MLT with a mixing length parameter $\ell/H_{\rm p}$ of 1.67, hydrogen burning was assumed to contribute 0.01% of the total luminosity (according to a nominal age of ≈3.6 Myr).

could also explain the long-term Doppler imaging observations for the RS CVn star HR 1099 by Vogt & Hatzes (1996) where some spots seemed to have emerged at low latitudes and then migrated towards the pole and merged with the polar spot. Also, the fact that several time-series Doppler-imaging studies yielded differential (surface) rotation in the opposite sense to that of the Sun, i.e. that the polar regions rotate faster than the equatorial region, allows some speculation in favor of the poleward migration scenario.

How does the surface map of HDE 283572 compare to other young and rapid rotators? The polar spot of HDE 283572 very much resembles the one seen on the rapidly rotating K0 ZAMS star AB Dor (e.g. Donati & Collier Cameron 1997) which is not only of comparable size and temperature difference but also of similar persistence despite having been reconstructed with a completely different imaging approach than applied in this paper. Four other K and G cluster ZAMS stars that were recently imaged by Barnes et al. (1998) and Stout-Batalha & Vogt (1996) also had a polar spot. One of them, the Pleiades G-type star HE 699, even appeared with a polar cap-like feature comparable in size to that of AB Dor and HDE 283572 while the others had a significantly smaller and strongly non-axisymmetric polar spot. We note though that these ZAMS stars are significantly faster rotators (P ≈0.5 days or ($50\Omega_\odot$), are less massive and older than HDE 283572.

A map of the early-type classical T Tauri star Sz68 by Johns-Krull & Hatzes (1997) showed cool starspots situated directly at the rotation pole while a map of the late-type classical T Tauri star DF Tau by Unruh et al. (1998) revealed mostly hot spots at low latitudes possibly due to an accretion shock close to the surface. Our previous study of the relatively faint WTTS V410 Tau had temperatures 600 K above and below the photospheric temperature while, on the contrary, our CFHT maps of the young, solar-type star LQ Hya (Strassmeier et al. 1993, Rice & Strassmeier 1998) revealed only cool surface features in the photosphere and possibly local velocity fields in the lower chromosphere but no (asymmetrically distributed) "hot" spots that could be interpreted as plages. Within the uncertainties of the atmospheric parameters of HDE 283572 in Table 2, we find no hot spots with $\Delta T > 100$ K from its photospheric absorption lines despite the fact that the Hα brightness is rotationally modulated with an amplitude of $0\overset{\rm m}{.}04\pm0\overset{\rm m}{.}01$ and in antiphase with the photospheric light. This behavior suggests the existence of chromospheric plages that are spatially related to the photospheric starspots. Many studies of main-sequence stars as well as of evolved stars reveal overwhelming evidence for the existence of bright chromospheric plages, most notably from the Mt. Wilson Ca II H&K survey, but also from direct map-

ping of absorption or emission lines (for example the enigmatic G2-giant FK Com by Piskunov et al. (1994) or for the RS CVn-type subgiant HU Vir by Strassmeier (1994)). The rotational modulation of the photospheric light of HDE 283572 is mostly due to the appendages of the polar spot at latitudes between +50° to +65° and suggests that the chromospheric plages on HDE 283572 are also located at high latitudes. Clearly, a search for rotational modulation of chromospheric and coronal activity indicators in this relatively bright star and its mapping would be quite rewarding.

Acknowledgements. KGS is very grateful to the Austrian Science Foundation (FWF) for support under grants S7301-AST (APT) and S7302-AST (Doppler imaging). JBR acknowledges support from the Natural Science and Engineering Research Council of Canada (NSERC). We thank Th. Granzer for computing the stellar and MHD models for us.

References

Barnes J. R., Collier Cameron A., Unruh Y. C., Donati J.-F., Hussain G. A. J., 1998, MNRAS, in press
Bertout C., Basri G., Bouvier J., 1988, ApJ 330, 350
Bouvier J., Covino E., Kovo O., Martin E. L., Matthews J. M., Terranegra L., Beck S. C., 1995, A&A 299, 89
Caligari P., Moreno-Insertis F., Schüssler M., 1995, ApJ 441, 886
Collier Cameron A., 1992, in Byrne P. B. & D. J. Mullan (eds.), *Surface Inhomogeneities on Late-Type Stars*, Lecture Notes in Physics, Vol. 397, Springer-Verlag, Berlin, p. 33
D'Antona F., Mazzitelli I., 1994, ApJS 90, 467
D'Antona F., Mazzitelli I., 1997, in Pallavicini R. & G. Micela (eds.), *Cool stars in clusters and associations*, Mem.S.A.It. 68, 4
Dempsey R. C., Neff J. E., Strassmeier K. G., Airapetian V. S., Lim J., 1999, ApJS, in prep.
DeLuca E. E., Fan Y., Saar S. H., 1997, ApJ 481, 369
Donati J.-F., Collier Cameron A., 1997, MNRAS 291, 1
Donati J.-F., Semel M., Carter B. D., Rees D. E., Collier Cameron A., 1997, MNRAS 291, 658
ESA 1997, The Hipparcos and Tycho catalog, ESA SP-1200
Fernández M., Miranda L. F., 1998, A&A 332, 629
Flower P. J., 1996, ApJ 469, 355
Frink S., Roeser S., Neuhäuser R., Sterzik M. F., 1997, A&A 325, 613
Gilroy K. K., 1989, ApJ 347, 835
Granzer Th., Schüssler M., Caligari P., Strassmeier K. G., 1999, A&A, in prep.
Gray D. F., 1992, in *The observation and analysis of stellar photospheres*, CUP, Cambridge
Grevesse N., Anders E., 1991, in Cox A. N. et al. (eds.), *Solar Interior and Atmosphere*, The Univ. of Arizona Press, Tucson, p. 1227
Hatzes A. P., 1995, ApJ 451, 784
Hatzes A. P., Kürster M., 1999, A&A, in prep.
Henry G. W., Fekel F. C., Hall D. S., 1995, AJ 110, 2926
Johns-Krull C. M., Hatzes A. P., 1997, ApJ 487, 896
Joncour I., Bertout C., Bouvier J., 1994a, A&A 291, L19
Joncour I., Bertout C., Menard F., 1994b, A&A 285, L25
Joy A. H.,1945, ApJ 102, 168
Kenyon S. J., Dobrzycka D., Hartmann L., 1994, AJ 108, 1872
Kürster M., Hatzes A. P., Pallavicini R., Randich S., 1992, in Giampapa M. S. & J. A. Bookbinder (eds.), $7th$ Cambridge Workshop on *Cool Stars, Stellar Systems, and the Sun*, PASPC 26, p. 249
Kurucz R. L., 1993, ATLAS-9, CD-ROM #13
Neuhäuser R., Wolk S. J., Torres G., et al., 1998, A&A 334, 873
Pavlenko Ya. V., Magazzú A., 1996, A&A 311, 961
Petrov P. P., Gullbring E., Gahm G. et al., 1995, in Strassmeier K. G. (ed.), Poster Proceedings IAU Symp. 176, *Stellar Surface Structure*, Univ. of Vienna, Vienna, p. 217
Piskunov N. E., Rice J. B., 1993, PASP 105, 1415
Piskunov N. E., Huenemoerder D. P., Saar S. H., 1994, in Caillault J.-P. (ed.), $8th$ Cambridge Workshop on *Cool Stars, Stellar Systems, and the Sun*, PASPC 64, p. 658
Preibisch T., Smith M. D., 1997, A&A 322, 825
Rice J. B., 1996, in Strassmeier K. G. & J. L. Linsky (eds.), IAU Symp. 176, *Stellar Surface Structure*, Kluwer, Dordrecht, p. 19
Rice J. B., Strassmeier K. G., 1996, A&A 316, 164 (paper II)
Rice J. B., Strassmeier K. G., 1998, A&A, in press (paper VII)
Rice J. B., Wehlau W. H., Khokhlova V. L., 1989, A&A 208, 179
Saar S. H., O'Neal D., Neff J. E., 1995, in Strassmeier K. G. (ed.), Poster-Proceedings IAU Symp. 176, *Stellar Surface Structure*, University of Vienna, Vienna, p. 105
Schmidt-Kaler T., 1982, in Landolt-Börnstein, Vol. I/2b, p. 15
Schüssler M., Caligari P., Ferriz-Mas A., Solanki S. K., Stix M., 1996, A&A 314, 503
Soderblom D. R., Jones B. J., Balachandran S., et al., 1993, AJ 106, 1059
Solanki S. K., Motamen S., Keppens R., 1997, A&A 324, 943
Stout-Batalha N. M., 1997, PhD Dissertation, University of California at Santa Cruz
Stout-Batalha N. M., Vogt S. S., 1996, in Strassmeier K. G. & J. L. Linsky (eds.), IAU Symp. 176, *Stellar Surface Structure*, Kluwer, Dordrecht, p. 337
Strassmeier K. G., 1994, A&A 281, 395
Strassmeier K. G., 1996, in Strassmeier K. G. & J. L. Linsky (eds.), IAU Symp. 176, *Stellar Surface Structure*, Kluwer, Dordrecht, p. 289
Strassmeier K. G., Bartus J., Cutispoto G., Rodonó M., 1997b, A&AS 125, 11
Strassmeier K. G., Bartus J., Kövari Z., Weber M., Washüttl A., 1998, A&A 336, 587 (paper VIII)
Strassmeier K. G., Boyd L. J., Epand D. H., Granzer T., 1997a, PASP 109, 697
Strassmeier K. G., Rice J. B., 1998, A&A 330, 685 (paper VI)
Strassmeier K. G., Rice J. B., Wehlau W. H., Hill G. M., Matthews J., 1993, A&A 268, 671
Strassmeier K. G., Welty A., Rice J. B., 1994, A&A 285, L17
Unruh Y. C., Collier-Cameron A., Guenther E., 1998, MNRAS 295, 781
Vogt S. S., Hatzes A. P., 1996, in Strassmeier K. G. & J. L. Linsky (eds.), IAU Symp. 176, *Stellar Surface Structure*, Kluwer, Dordrecht, p. 245
Vogt S. S., Hatzes A. P., Misch A., Kürster M., 1998, ApJS, in press
Vogt S. S., Penrod G. D., Hatzes A. P., 1987, ApJ 321, 496
Walter F. M., Brown A., Linsky J. L. et al., 1987, ApJ 314, 297